International Journal of Automotive Technology, Vol. 7, No. 4, pp. 415–422 (2006)

1229–9138/2006/028–05

LARGE EDDY SIMULATIONS OF TUMBLE AND SWIRL FORMATIONS IN ENGINE IN-CYLINDER FLOW

B. S. LEE and J. S. LEE*

School of Mechanical & Aerospace Engineering, Seoul National University, Seoul 151-742, Korea

(Received 23 November 2005; Revised 31 January 2006)

ABSTRACT–Swirl and tumble flows in an engine in-cylinder have been simulated by using a three-dimensional computational fluid dynamics code, and the results are validated in comparison with experimental data. The large eddy simulation based on the Smagorinsky model and the fractional step method is adopted to describe the turbulence of in-cylinder flows and to save computing time, respectively. The main purpose of this study is connected with the effect of various conditions of intake flows on formation and development of in-cylinder tumble and swirl motions. The engine speeds considered are 1000 rpm and 3000 rpm for intake flows with inclination angles between –10° and 20° at deflection angles of 0°, 22.5°, and 30°. The results are discussed by visualizing flow fields and by evaluating parameters in relation to vortex intensity such as swirl and tumble ratios.

KEY WORDS : Large eddy simulation, Tumble and swirl motions, Inclination and deflection angles of intake flow

1. INTRODUCTION

The in-cylinder flows of internal combustion (IC) engines have drawn much attention because the flow structure generated by intake flows is related closely to the design and performance of the IC engine. The generation of high turbulence intensity is one of the most important factors for stabilizing the ignition process and fast propagation of flame, especially in the case of lean-burn combustion. In general, two types of vortices are utilized in order to efficiently generate and preserve turbulence. The vortices are usually called swirl and tumble which are organized rotations in the horizontal plane and in the vertical plane of the engine cylinder, respectively. They contribute to the enhancement of engine performance by accelerating mixing of fuel and induced air (Heywood, 1988). It is thus indispensable for the development of an IC engine with high compression ratio (CR) to realize high turbulence intensity and lean burn combustion.

Quite a few experiments of in-cylinder flows have been conducted to measure velocity fields and turbulence intensities by using the hot wire anemometry or laser Doppler velocimetry (Stone, 1992). However, it is a really hard task because in-cylinder flows in the reciprocating engine are characterized by highly complex three-dimensionality, turbulence and unsteadiness. A numerical approach could thus be an alternative because of the capability of computational fluid dynamics (CFD) which has been developed for in-cylinder flow predictions in recent 20 years. Gosman's work (1986) can be regarded as a pioneering one which applied CFD to simulate in-cylinder flows, and since then tremendous improvements have been achieved in computational techniques. The KIVA and STAR-CD are most frequently used as commercial package programs for flows in the reciprocating engine in these days. Most recently, Haworth and Jansen (2000) have conducted large eddy simulations (LES) in order to more accurately describe the turbulence structure resulting from the complex geometry.

The present study aims to figure out controlling geometric parameters, which is necessary in the design of the efficient intake flow system by analyzing the LES results, and to identify the effects of various intake and operating conditions. Above all, in the development of the LES computer code to improve the accuracy, a four-step time advancement scheme of the fractional step method is implemented to save the computing time. Firstly, it is attempted to simulate flows in a simple engine with one intake port and to validate the code by comparing the results with experimental data. And then, a model engine with two intake valves (a four-valve system) is considered. In the two-valve system that has only one intake port, it is relatively easy to conserve swirling generated by helical ports because the swirl develops along the rotational axis. On the other hand, it is difficult to conserve swirling for the four-valve system because the

*Corresponding author. e-mail: jslee123@snu.ac.kr

swirl flows generated by two helical ports interfere with each other. Thus, tumble is considered as a more important mechanism than swirl for these systems. The gasoline direct injection (GDI) engine that draws much attention recently makes use of the tumble mechanism (Kamura and Takada, 1998). Hence, the present LES focuses on the generation and growth of both tumble and swirl motions under various in-flow conditions.

2. NUMERICAL METHOD

2.1. Governing Equations

Governing equations are formulated in the cylindrical coordinate system (r, θ, z) as shown in Figure 1. The continuity and momentum equations can be expressed in a conservative form as follows;

$$\frac{\partial(\rho\phi)}{\partial t}+\frac{1}{r}\frac{\partial}{\partial t}\left(r\rho u_r\phi-r\Gamma_\phi\frac{\partial\phi}{\partial r}\right)$$

$$+\frac{1}{r}\frac{\partial}{\partial\theta}\left(\rho u_\theta\phi-\frac{\Gamma_\phi}{r}\frac{\partial\phi}{\partial\theta}\right) \quad (1)$$

$$+\frac{\partial}{\partial z}\left(\rho u_z\phi-\Gamma_\phi\frac{\partial\phi}{\partial z}\right)=S_\phi$$

where ϕ represents dependent variables, Γ_ϕ is the diffusivity coefficient of variable ϕ, and S_ϕ denotes the source term. For the continuity equation, ϕ is set to 1, and for momentum equations, it represents one of three velocity components (u_r, u_θ, u_z). In the simulation, the z-coordinate is transformed to the x-coordinate in such a way that $\xi = z/z_p$, where z_p is the location of the piston, so that the moving boundary of the piston head can be treated with ease. The transformed equations can be expressed as

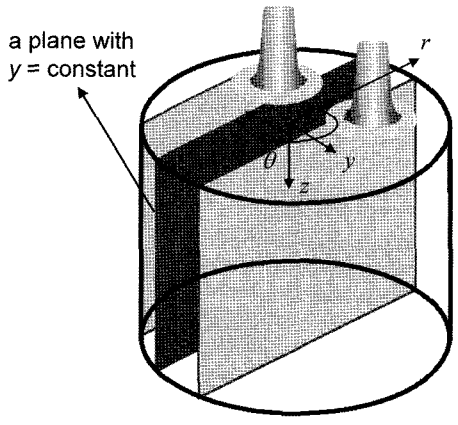

Figure 1. Engine cylinder configuration in cylindrical and Cartesian coordinates.

$$\frac{1}{z_p}\frac{\partial(\rho z_p\phi)}{\partial t}+\frac{1}{r}\frac{\partial}{\partial r}\left(r\rho u_r\phi-r\Gamma_\phi\frac{\partial\phi}{\partial r}\right)$$

$$+\frac{1}{r}\frac{\partial}{\partial\theta}\left(\rho u_\theta\phi-\frac{\Gamma_\phi}{r}\frac{\partial\phi}{\partial\theta}\right) \quad (2)$$

$$+\frac{1}{z_p}\frac{\partial}{\partial\xi}\left(\rho\tilde{u}_z\phi-\Gamma_\phi\frac{1}{z_p}\frac{\partial\phi}{\partial\xi}\right)=S_\phi$$

where $\tilde{u}_z$ is the relative axial velocity with respect to the moving grid, which is given by

$$\tilde{u}_z=u_z-u_g \quad (3)$$

where u_g is the axial velocity of the moving grid.

To reduce excessive computing time, which has been one of most serious problems in CFD of engine in-cylinder flow, the fractional step method (Choi and Moin, 1994) is adopted to obtain solution to Equation (2), because the fractional step algorithm is especially more efficient for unsteady problems than the conventional SIMPLE algorithm.

2.2. Sub-grid Scale Model

The basic idea of LES stems from two experimental observations. Firstly, the large-scale structure of turbulent flows varies greatly from flow to flow, and is consequently difficult, if not impossible, to model in a general way. Secondly, the small-scale turbulence structures are nearly isotropic, very universal in character, and hence much more amenable to the general modeling. If the criterion to divide the two scales is Δ, the large scaled velocity can be filtered as follows;

$$\bar{u}_i=\int G(x_i,x_i':\Delta)u_i(x_i)dx_i' \quad (4)$$

where G is the Gaussian cut-off function. Here the influence of unresolved (subgrid-scale) motions on the resolved scales is treated as additional viscosity so that the effective stress, τ_{ij}, can be regarded as the sum of viscous stress, τ_L, and sub-grid scale stress, τ_{SGS}. Then, it follows that

$$\tau_{ij}=\tau_{L,ij}+\tau_{SGS,ij} \quad (5)$$

In this study, the Smagorinsky sub-grid scale (SGS) model (Germano *et al.*, 1991) is employed, which can be expressed as

$$\tau_{SGS,ij}=-2\nu_{SGS}\bar{S}_{ij}=-2\nu_{SGS}\left(\frac{\partial\bar{u}_i}{\partial x_j}+\frac{\partial\bar{u}_j}{\partial x_i}\right) \quad (6)$$

Here $\bar{S}_{ij}$ is the rate of strain tensor, $\bar{u}$ is the filtered velocity and $\nu_{SGS}=(C_s\Delta)^2(2\bar{S}_{ij}\bar{S}_{ij})^{1/2}$ where C_s=0.01 is the Smagorinsky constant.

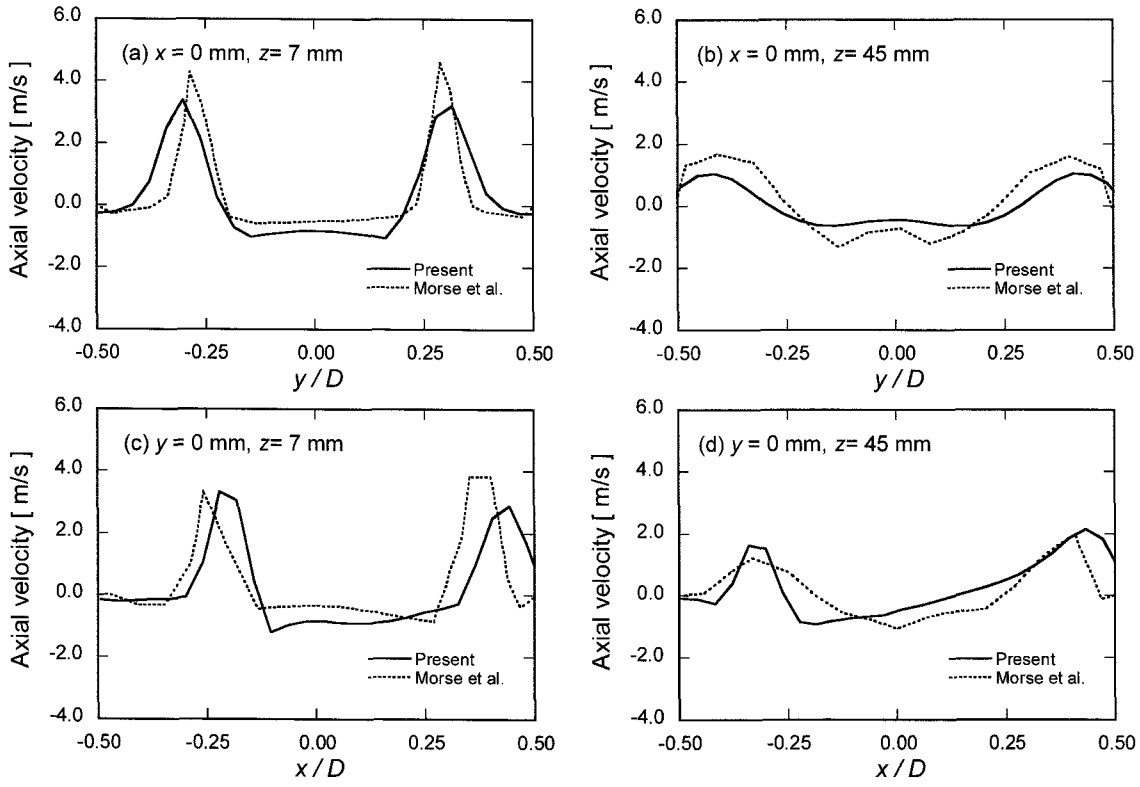

Figure 2. Axial velocity profiles at 90° ATDC.

3. RESULTS AND DISCUSSION

3.1. Motoring Engine with One Valve

To confirm the validity of the developed computer code, the predicted results for a motoring engine with one valve are compared with experimental data of Morse *et al.* (1980). The motoring engine, which has a disc chamber and an off-center intake port, operates at a low speed of 200 rpm with 60° seat angle, 75 mm in bore diameter, 0.8 stroke-to-bore ratio, and compression ratio of 3. The valve center is located at $x = 8$ mm in Figure 1. Figures 2(a) and 2(b) show axial velocity profiles along the y direction at two different axial locations, $z = 7$ and 45 mm, in the y-z plane at 90° ATDC (After Top of Dead Center), and Figures 2(c) and 2(d) correspond to those along the x direction in the x-z plane. The present simulation follows fairly well the general trend of experimental data considering the measurement uncertainties. The two peaks in the axial velocity profile in Figure 2(a) are due to the air jets induced from the intake valve with 60° seat angle, and are smoothed away by shearing as moving downward at $z = 45$ mm (Figure 2(b)). In the x-z plane (Figures 2(c) and 2(d)), the velocity profile does not show symmetry because the valve is located off from the center of the cylinder top wall by $x/D = 0.107$, which is about the center of two local peaks as shown in Figure 2(c). The two peaks in the velocity profile spread toward the cylinder side wall as moving downward to $z = 45$ (Figure 2(d)).

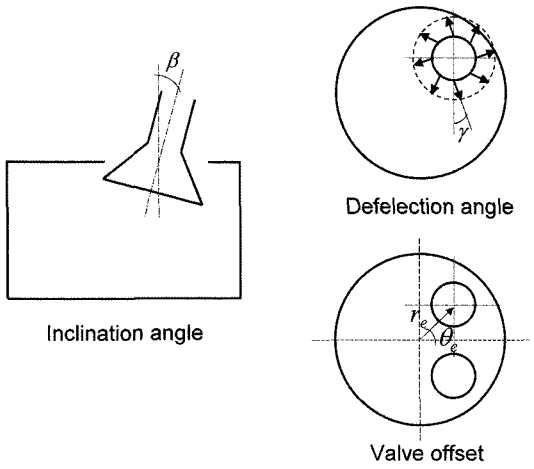

Figure 3. Schematic of the model engine.

3.2. Model Engine with Two Intake Valves

The configuration of the real engine with a four-valve system is simplified as a model engine as shown in Figure 3, where the intake valve geometries and in-flow

Table 1. Engine specification.
(λ = length ratio of conneticng rod to crank radius)

Engine		Valve	
Bore	83 mm	Diameter	29 mm
Stroke	92 mm	Seat angle	60°
CR	9.0	r_e	19 mm
λ	3.0	θ_e	45°

conditions are described. The detailed specifications of the model engine are listed in Table 1. The present simulations focus on the effects of three parameters such as the inclination angle β, deflection angle γ, and engine speed on in-cylinder flow fields. The inclination angle can be regarded as an approximate measure of the jet direction induced by the intake port, and the deflection angle is related closely to swirl flow that is induced by helical ports. To investigate the effects of these angles, simulations are conducted for inclination angles from −10° to 20°, and three deflection angles of 0°, 22.5° and 30°. In addition, the engine speeds considered are 1000 rpm and 3000 rpm. The grid system used is 30 × 32 × 20 in (r, θ, z) directions, and the time steps are chosen as Δt = 0.1 ms to take 600 time steps per one revolution for 1000 rpm and Δt = 0.025 ms to take 800 time steps for 3000 rpm.

In order to quantitatively evaluate the vortex intensity, the normalized swirl and tumble ratios are defined as the angular momentum of the flow about a specified axis divided by the moment of inertia of the in-cylinder flow about that axis. It is normalized by the angular speed of the crankshaft. The angular momentum, H_i, and the moment of inertia, M_i, are evaluated, respectively, by

$$H_i = \int_{V(t)} \rho \vec{r} \times \vec{u} \cdot \vec{n}_i dV, \quad M_i = \int_{V(t)} \left| \rho \vec{r} \times \vec{n}_i \right|^2 dV \tag{7}$$

where ρ is gas density, $\vec{r}$ and $\vec{u}$ are position and velocity vectors, respectively. $\vec{n}_i$ is an i-component unit vector where i indicates x, y, or z, and V denotes the cylinder volume.

The swirl and tumble ratios are normalized as follows;

$$S = H_z/M_z\omega, \; T_x = H_x/M_x\omega, \; T_y = H_y/M_y\omega \tag{8}$$

where S is the swirl ratio, T_x and T_y are the tumble ratios about x and y axes, respectively, and ω is the speed of the crank shaft.

3.2.1. Tumble motion in the model engine

In order to efficiently visualize generation and development of the tumble flow, the velocity vector fields in the x-z plane at y = −20 mm are depicted in Figure 4 at different ATDC, when β = 0°, γ = 0°, and the engine speed is 1000 rpm. This figure illustrates how the tumble motion is generated and developed with time. The plane at y = −20 mm is apart long from the center where two air jets from the valves collide with each other and attenuate as time goes by. Two tumbles are generated in the initial stage as shown in Figure 4(a), that is, a strong tumble beneath the intake port and a weak one on the left. The strong tumble is generated because the air jets through the intake port collide with the piston head and turn their direction along the wall of the piston head. However, this tumble diminishes before 90° ATDC because the room needed to develop narrows down, which is suppressed by growth of the other tumble. The weak tumble on the left is induced initially due to shearing with the strong tumble but survives until the end of the expansion process. The tumble intensity increases as the piston moves down and the cylinder volume expands as shown in Figures 4(b)-(d).

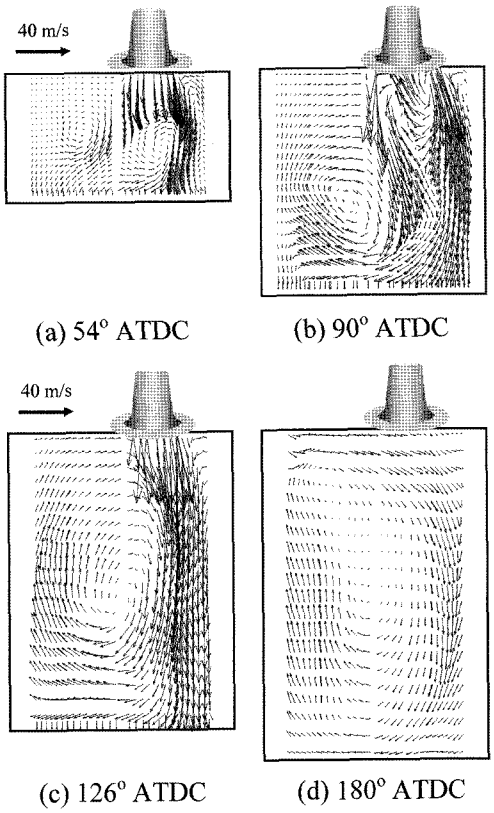

Figure 4. Velocity distributions in x-z plane for various crank angles when β = 0°, γ = 0° at y = −20 mm, Engine speed is 1000 rpm.

Now the effect of inclination on the tumble intensity is discussed by observing the tumble flow fields and the tumble ratio according to the change of inclination angles. Figures 5 and 6 show flow fields in the x-z plane

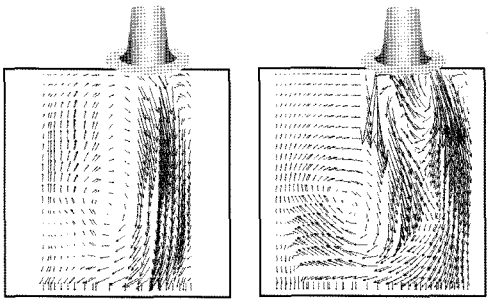

(a) $y = -30$ mm (b) $y = -20$ mm

Figure 5. Velocitry distributions at 90° ATDC, $\beta = 0°$, $\gamma = 0°$. Engine speed is 1000 rpm.

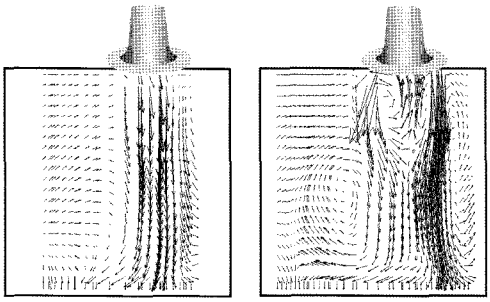

(a) $y = -30$ mm (b) $y = -20$ mm

Figure 6. Velocitry distributions at 90° ATDC, $\beta = 20°$, $\gamma = 0°$. Engine speed is 1000 rpm.

at $y = -30$ mm and -20 mm at 90° ATDC for $\beta = 0°$ and 20°, respectively, when the engine speed is 1000 rpm. As can be seen in these figures, the tumble intensity appears weak at the larger inclination angle under the configuration of 60° seat angle. The reason is that the jet flow induced from the intake valve flows more in parallel with the cylinder side wall in the case of 60° seat angle.

For other cases with different inclination angles, the effect is presented in terms of the tumble ratio to quantify tumble intensities in Figure 7. In general, the tumble intensity increases with ATDC until it reaches its maximum at about 150° ATDC regardless of the inclination angle, and then decreases afterwards. It is clearly seen that the absolute value of the tumble ratio gradually decreases as the inclination angle increases. The case of 0° inclination can be regarded as an optimal condition with a view point of tumble generation for the jet flow with 60° seat angle because the jet flow from the valve inlet collides more obliquely with the cylinder side wall. As the inclination angle increases, the direction of the jet issued at the valve inlet is getting parallel to the cylinder side wall as can be seen in Figures 5 and 6, which results in low tumble intensity. It can thus be inferred that the seat angle and inclination angle are

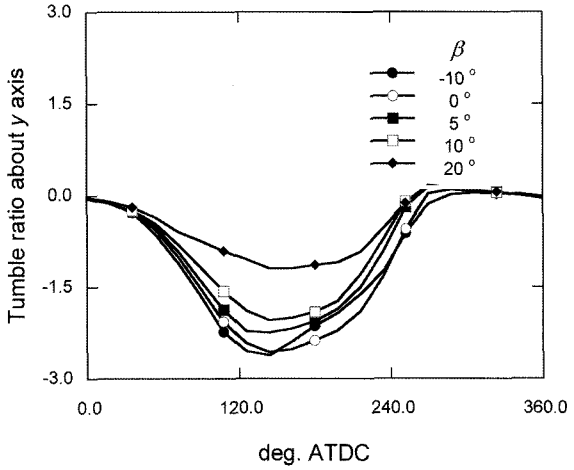

Figure 7. Time change of T_y at various inclination angles at $\gamma = 0°$. Engine speed is 1000 rpm.

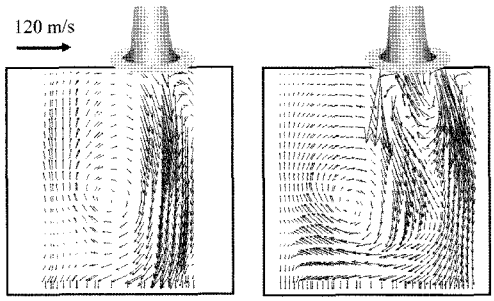

(a) $y = -30$ mm (b) $y = -20$ mm

Figure 8. Velocitry distributions at 90° ATDC, $\beta = 0°$, $\gamma = 0°$. Engine speed is 3000 rpm.

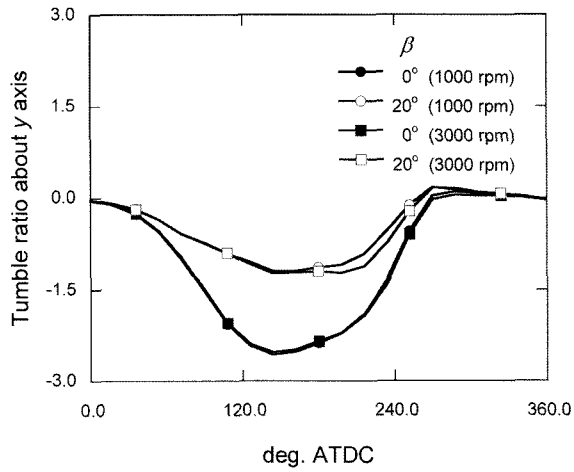

Figure 9. Variation of T_y with crank angle at $\gamma = 0°$.

important factors to activate the tumble formation.

Figure 8 shows the velocity vectors at the engine speed of 3000 rpm under the same operating and inflow

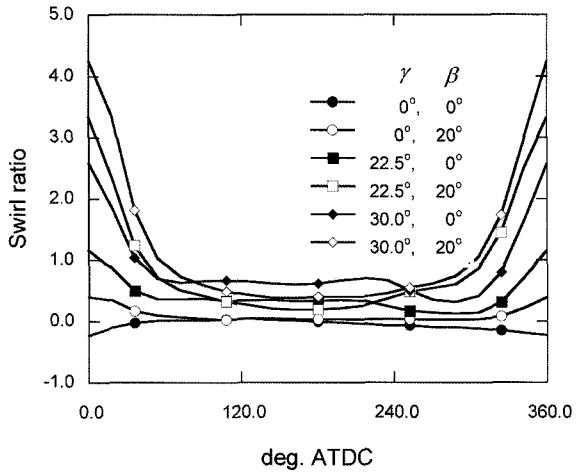

Figure 10. Variation of swirl ratio with crank angle at 1000 rpm.

conditions as those in Figure 5. No significant difference is observed in the flow structure, comparing with the tumble flow at 1000 rpm except the increase in the velocity magnitude. Note that the magnitude of velocity vector is scaled down to one third of that at 1000 rpm.

The normalized tumble ratios at two different engine speeds shown in Figure 9 support the weak dependence of the engine speed on flow structures. In this cold flow simulation with coarse grid, complex phenomena such as high compression, fast explosion, and combustion are not reflected on the effect of the engine speed, however, it seems that the tumble data at the low engine speed can be a guide line for those at the high engine speed.

3.2.2. Swirl motion in the model engine

In two intake valve systems, it is difficult to preserve a single swirl rotating about the same axis even if the induced air flows are artificially made to possess swirl components because two induced air flows with different rotating axes are inclined to collide with each other, which make the swirl flow weaker. Figure 10 shows swirl ratio variations according to ATDC at different inclination and deflection angles when the engine speed is 1000 rpm. The swirl ratios are nearly constant or small in the magnitude in the region from 80° to 280° ATDC, but an abrupt increase is observed in other regions when the deflection angles are large as shown in Figure 10. The swirl ratio is dominantly affected by intake flow fields, that is, by the deflection angle γ near the top of the dead center, but the induced swirl flows decay and return to low value as they proceed to the piston head as time goes by. When $\gamma = 0°$, no swirl is practically induced regardless of the inclination angle. The swirl ratio increases with the deflection angle, and it has larger value when the inclination angle is 20° for a given deflection angle in the region where ATDC < 80° and ATDC > 280°. However, in the region from 80° to 280° ATDC, the swirl ratio is larger when the inclination angle is 20°.

Considering the fact that the swirl ratio is meaningful only in the region from 80° to 280° ATDC because the swirl should be preserved in this region for effective combustion, the inclination angle of 0° is more preferable than 20°. Although the swirl ratio could be enhanced when the induced swirling is augmented at the cost of flow friction due to the use of the helical port, the outcome would still be unsatisfactory in comparison with the effect on one intake port engines (Wakisaka *et al.*, 1986). Even the maximum value of the swirl ratio in the region from 80° to 280° ATDC doesn't reach unity. It can thus be concluded that the swirl ratio has inherently low value in two intake valve systems despite the induced swirl, and the deflection angle can not make a considerable contribution in enhancing the swirl ratio.

3.2.3. Interaction between tumble and swirl

In this section, it is intended to describe how swirl and tumble interact with each other in their generation and growth. It can effectively be examined by considering the effect of the deflection angle on the tumble motion, and the effect of the inclination angle on the swirl motion, which are regarded as independent pairs of parameters.

Figure 11 shows flow fields in 3 pairs of x-z planes cut by $y = \pm 10$, ± 20 and ± 30 mm. The engine is operated at 1000 rpm with no inclination but deflection angle of 30°. As can be seen in the figure, the flow symmetry about $y = 0$ is broken down in both swirl and tumble motions because of the deflection angle. Moreover, the tumble in

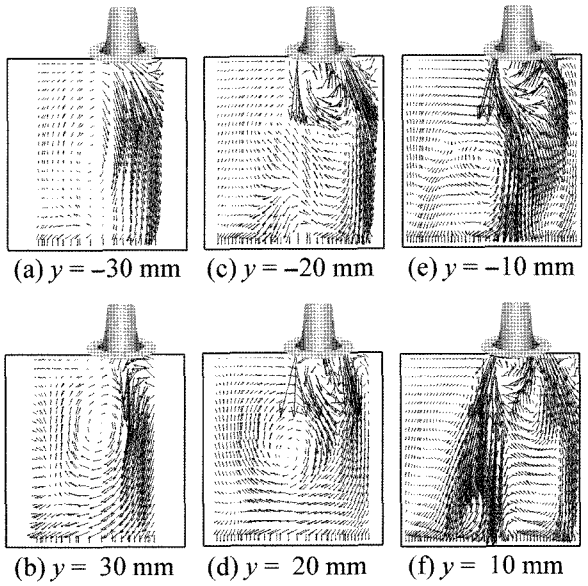

Figure 11. Velocity distributions at various crank angles at $\beta = 0°$ and $\gamma = 30°$. Engine speed is 1000 rpm.

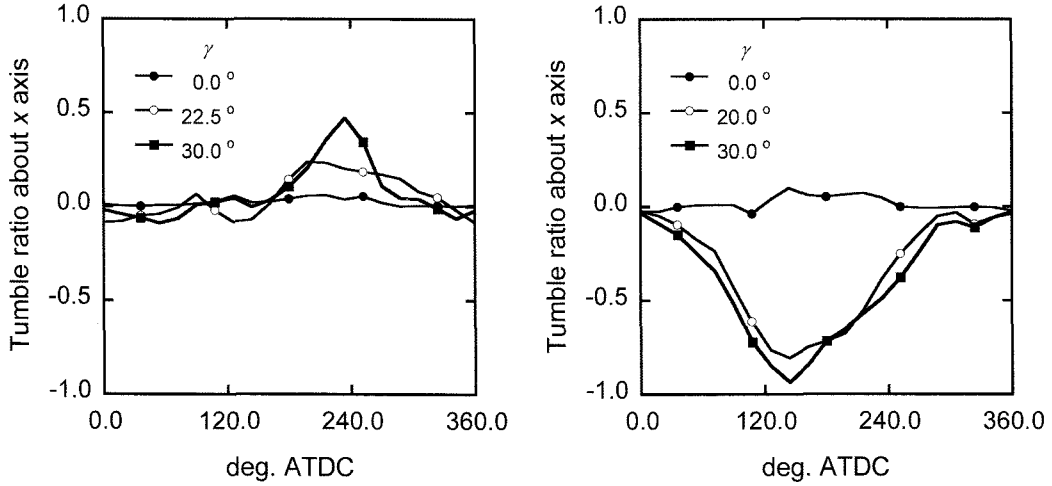

Figure 12. Variation of Tumble ration about x axis with γ

the planes at the positive y location is developed much stronger than that in the swirls, which are induced by the intake valves and regulated planes at the negative y location. This is because the two swirls, which are induced by the intake valves and regulated by the deflection angles, interact with the cylinder wall in different ways. One swirl in the plane at the positive y location is promoted by the wall, while the other one in the negative y location is blocked by the wall because the swirls have different walls with which they collide, while they have the same rotating directions.

In Figure 12, the tumble ratio variation about the x axis with time is represented for 3 different deflection angles. The value of the tumble ratio about the x axis, T_x, is small compared to that about the y axis, T_y, shown in Figure 7. The tumble is negligible when the deflection angle is 0°

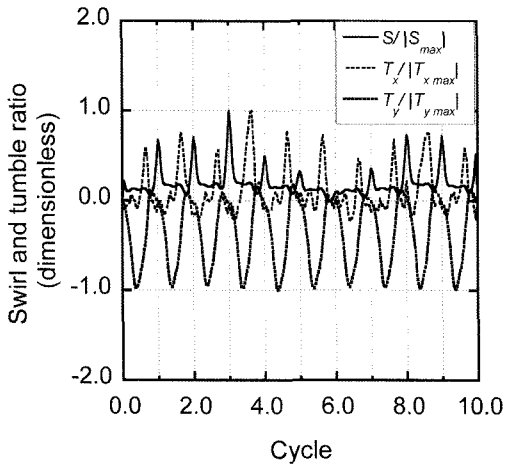

Figure 13. Cyclic variation of swirl and tumble ratio at β = 0° and γ= 30°. Engine speed is 1000 rpm.

even in the case that β= 20°. However, the value increases to the same order of T_y as the deflection angle increases. Accordingly, the induced swirl should not be treated lightly in design though it can directly develop to the stabilized swirl in two intake valve systems. Therefore, swirl and tumble of intake flows must be adjusted properly for faster internal combustion.

3.2.4. Cycle-to-cycle variation

Differently from RANS (Reynold averaged Navier-Stokes), the ensemble-averaged mean velocities over ten cycles are presented in the previous sections. However, all the instantaneous properties of the flow is affected by cycle-to-cycle variation. Figure 13 shows the swirl and tumble ratios over ten cycles in the case with γ= 30° and β= 0°. Different maximums or minimums are observed in the figure for the three rotational properties. Since the tumble about the y axis has the largest intensity for this engine, the cycle-to-cycle variation is small compared with others. The small vortices related with S and T_x are sensitive to the cycle-to-cycle variation.

4. CONCLUSIONS

In this work, a three-dimensional CFD program was developed to perform computations of in-cylinder flows of a model engine with two intake valves after validation procedure by comparing with experimental data. The program is based on LES with Smagorinsky model and the fractional step method to describe the turbulence of in-cylinder flows and to save computing time.

Two tumbles having axis of rotation in the y direction are generated but only one tumble survives until the end of expansion. This single tumble is thought to be an important mechanism to support stabilized combustion

because of the durability and single direction. The factors, which affect the direction of the induced jet flow, such as seat angle and inclination play important roles in generation and development of the tumble about y axis because the generation of tumble can be obstructed depending on the direction of the induced jet from intake valves. The tumble intensity decreases as inclination angle increases from $-10°$ to $20°$ at $60°$ seat angle.

Although the swirl intensity of the induced swirl appears low for two intake valve systems, the induced swirl shows a considerable effect on tumbles about both x and y axes. The low intensity swirl motion can bring about destruction of tumbles. In the presence of the induced swirl, tumble intensities about the y axis are high in the region of positive y but low in the negative y region. As the induced swirl increases, the intensity of tumble about the x-axis increases from negligible level to the same order of the tumble about the y-axis.

REFERENCES

Choi, H. and Moin, P. (1994). Effects of the computational time step on numerical solutions of turbulent flow. *J. Comp. Phys.*, **113**, 1–4.

Germano, M., Piomelli, U., Moin, P. and Cabot, W. H. (1991). A dynamic subgrid-scale eddy viscosity model. *Phys. Fluids A*, **3**, 1760–1765.

Gosman, A. D. (1986). Flow processes in cylinders. *The Thermodynamics and Gas Dynamics of Internal Combustion Engine,* **II**, edited by J. H. Horlock and D. E. Winterbone, Oxford University Press. New York.

Haworth, D. C. and Jansen, K. (2000). Large eddy simulation on unstructured deforming meshes: Towards reciprocating IC engines. *Computers and Fluids*, **29**, 493–524.

Heywood, J. B. (1988). *Internal Combustion Engine Fundamentals, Int. Edn.*, McGraw-Hill Inc. New York.

Kamura, H. and Takada, K. (1998). Development In-cylinder gasoline direct injection engine. *JSAE Review*, **19**, 175–180.

Morse, A. P., Whitelaw, J. H. and Ylanneskis, M. (1980). The flow characteristics of piston-cylinder assembly with an off-centre, open port. *Proc. IMechE*, **194**, 291–299.

Stone, R. (1992). *Introduction to Internal Combustion Engines.* 2nd Edn., The Macmillan Press Ltd. Londons.

Wakisaka, T., Shimamoto, Y. and Isshiki, Y. (1986). Three-dimensional analysis of in-cylinder flows in reciprocating engines. *SAE Paper No.* 860464.